Available online at www.sciencedirect.com
ScienceDirect
Journal of Sound and Vibration 318 (2008) 549–564
JOURNAL OF SOUND AND VIBRATION
www.elsevier.com/locate/jsvi

Experiments on routes to chaos in ball bearings

B. Mevel[a,*], J.L. Guyader[b]

[a]S.N.R. Roulements, 1 rue des usines, F74010 Annecy, France
[b]Laboratoire Vibrations-Acoustique, I.N.S.A. de Lyon, 20 Avenue A. Einstein, F69621 Villeurbanne Cedex, France

Received 28 May 2006; received in revised form 10 April 2008; accepted 10 April 2008
Handling Editor: M.P. Cartmell
Available online 10 June 2008

Abstract

The theoretical motion of a ball bearing has been studied in a previous paper. Using a control parameter, different routes to chaos were described. The aim of this paper is to study the experimental routes to chaos in a ball bearing and to confirm whether theoretical predictions of the phenomena are realistic.

An experimental test bench has been used and a numerical procedure has been proposed for observing Poincaré maps. As the control parameter varies the bearing clearly shows the appearance of instability in its motion. Two different routes to chaos are described as expected from the theory.

The first route is related to the first resonant frequency of the bearing. It is a sub-harmonic route. The second route, associated with the second resonant frequency, is a quasi-periodic route.

1. Introduction

Experiments in ball bearings are important for validating theories and bearing behaviour. To many users a ball bearing is considered as a black box containing balls, one ball retainer, some lubricant and sometimes seals. All parts are rotating except for one ring. Bearings are present in almost all rotating systems and are unknown to users unless something goes wrong. This is an interesting field for research to develop predictive methods to warn users before any damage in the case of bearing failure. An important literature deals with bearing responses in condition monitoring in machines. In Refs. [1,2], the bearings vibrations are not only evaluated by Fourier spectrums and mean values but also with characteristic tools used in nonlinear dynamics such as phase portraits and Poincaré sections. An advanced work in this paper is to use these same tools to quantify the vibration levels and to analyse the internal dynamics of a ball bearing. The understanding of ball bearing behaviour implies a good knowledge of the load distribution of rolling element bearings, contact angles and the contact pressures between balls and raceways.

Some arrangements for analysing the internal behaviour of ball bearings are well known. The simplest method is to apply a thin copper layer onto the race-way, and then run the bearing for a short time under the desired load. After completely dismantling the bearing assembly the challenge is then to analyse the state of

*Corresponding author. Tel.: +33 450653169; fax: +33 450653033.
E-mail addresses: bruno.mevel@snr.fr (B. Mevel), jean-louis.guyader@insa-lyon.fr (J.L. Guyader).

0022-460X/$ - see front matter © 2008 Elsevier Ltd. All rights reserved.
doi:10.1016/j.jsv.2008.04.024

the remaining copper layer. The circumferential shape of the uncovered steel is an indication of the contact path. From this, the maximum loads and the unloaded area can then be located. In this experiment, the contact slip generates local wear of the materials. This wear depends on the traction coefficient that is a property of the lubricant but also the local temperature. In such experiments, one may obtain uncertain shapes and therefore the conclusions are not straightforward. A completely different method would be to modify parts of the bearing. A transparent and plastic outer ring is a useful way to obtain interferometry patterns which are characteristic of contact loads. This kind of analysis is specifically used to determine contact stresses. Finally, it is clear that there are still challenges in analysing the internal behaviour of bearings.

Fortunately, the safe dynamic motion of ball bearings is the most common behaviour encountered in industry. Fittings and loads are applied to the bearings and are generally appropriately defined in order to avoid high levels of vibrations, unexpected instabilities and low levels of reliability. In case the loads and fittings are not correctly set, the vibration level increases and the dynamic motion of the ball bearing becomes complicated.

Theoretical studies of bearing behaviour started in the early 1950s. At this time only quasi-static analysis was possible. Inertia and damping were neglected but the influence of clearance and loads was clearly stated. A kinematic study was proposed by Sunnersjo [3] who showed that vibration levels depended on inertia and speed. Some experiments were carried out to validate the proposed theory. The influence of the type of loads, radial clearance and rotational speed was then clearly demonstrated.

A nonlinear model of a ball bearing subject to a constant radial load was proposed by Fukata et al. [4]. It shows the influence of the rotating speed. Chaos-like, super-harmonic and sub-harmonic motions were analysed using time series and Poincaré maps. An increase of vibration levels around two specific rotation speeds was also noticeable.

In Ref. [5] a nonlinear model of a ball bearing with five degrees of freedom was proposed to study its stiffness under different kinds of loading. A three degree of freedom model was used in Ref. [6] and quasi-periodic and sub-harmonic routes were reported. In Ref. [7], a two degree of freedom model was used to simulate a radially loaded bearing. By modifying the damping factors of the model, different routes to chaos were noticeable and related to critical speeds of the ball bearing. Around the first critical speed the ball bearing shows instability and generates sub-harmonics of the ball pass frequency. Using the damping factor as a control parameter, it is possible to reach a chaotic region after an infinite number of bifurcations. Around the second critical speed, some combinations of the second resonant frequency and the ball pass frequency occur and generate a quasi-periodic motion. As the internal damping factor of the bearing decreases, the number of combinations of the two basic frequencies increases and rapidly overlaps, resulting in chaotic motion. Finally, the introduction of some over-sized balls in the bearing generates chaotic motions; this route was called the intermittent-like route.

A more recent study of the different kinds of motions in a nonlinear ball bearing model was proposed by Harsha in Ref. [8]. The bearing behaviour was studied with different levels of load and speed. The observations were similar to those in Ref. [7] with periodic, sub-harmonic and quasi-periodic Poincaré maps.

To describe these strange motions, tools specific to chaotic dynamics have to be introduced [9–11]. Fourier spectra are convenient for detecting sub- or super-harmonics of a component, also in the case of complete chaotic behaviour, but the quasi-periodic motion is impossible to detect except for the ideal case of two incommensurate components. Some recent studies, not associated with bearing motion, have used phase planes and Poincaré sections. The former just plots displacements as a function of themselves or their derivative. An extremely efficient technique is then to sample the phase plane points using a convenient clock frequency, in order to obtain a limited number of points. The resulting shape is an excellent tool to characterise sub-harmonic, quasi-periodic or chaotic motions.

Most studies introduced here are merely theoretical, and a lack of experiments is noticeable. An interesting paper, [12], deals with an experimental study of bearings in a rotor system. The work reported did not show chaotic behaviour but a period-doubling phenomenon is obvious.

The work of Ghafari et al. [1] confirmed the existence of chaos in healthy bearings, and the potential of chaos tools for the diagnosis of faults in rotating machinery. Another interesting paper is [2] in which faulty bearings are analysed using Poincaré maps. These are indications that the theoretical chaos tools provide an opportunity to demonstrate their power in industrial applications.

As a continuation of Ref. [7], an experiment was carried out in this paper to confirm our predictions of routes to chaos in ball bearings. The experiment is based on a test rig specially dedicated and an experimental procedure to generate projection of attractors. This paper presents the main results of this experiment.

2. Bearing modelling

The following bearing modelling was derived in Ref. [7] to study the routes to chaos and here provides guidelines to design the experimental set-up. The resolution of the following equations allows us to calculate the mass displacements permitting comparisons with experiments.

2.1. Equation of motion

As shown in Fig. 1, an ideally radially loaded ball bearing is considered. The two rings are rigid bodies and so the raceways may be represented by two circles. The balls are assumed to be massless, the inner ring has no translation but rotates around its axis z and the outer ring has two translations x_e and y_e in its plane but no rotation about its axis z. The equation of motion of the outer ring is

$$Mx_e''(t) + Cx_e'(t) + \sum_{j=1}^{Z} f_j(t)\cos(\theta_j(t)) = F \tag{1}$$

$$My_e''(t) + Cy_e'(t) + \sum_{j=1}^{Z} f_j(t)\sin(\theta_j(t)) = 0 \tag{2}$$

where $\theta_j(t) = \theta(t) + (j-1)2\pi/N$ is the angular position of the jth ball, $\theta(t)$ is the angular position of the rotating frame associated with the ball retainer and $f_j(t)$ is the load associated with the jth ball. C is the damping coefficient taking into account different dissipation phenomena that are not included in the model. Its value is generally about 30% of the critical damping value. The loads $f_j(t)$ are calculated by the Hertz formula:

$$f_j(t) = K\delta_j(t)^{3/2} \tag{3}$$

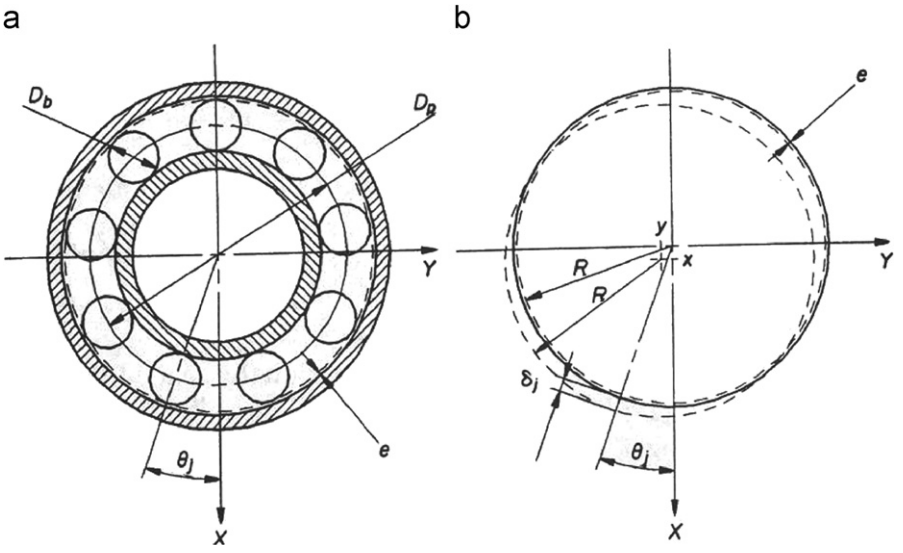

Fig. 1. (a) Bearing geometry and (b) modelling.

where K is a contact coefficient which is a function of the Young modulus of the contacting parts and of their local curvatures and δ_j is an approximation of the distance between the two circles along the θ_j direction:

$$\delta_j(t) = x(t)\cos\theta_j(t) + y(t)\sin\theta_j(t) - e \tag{4}$$

2.2. Ball bearing varying compliance (VC)

The stiffness of a radially loaded ball bearing is a function of the relative displacement of its inner and outer ring, i.e. a function of the load applied to the bearing and the resulting equilibrium but also as a function of the position of the balls. As the balls move in and out of the loaded area, the rigidity of the bearing varies, and follows a periodic curve. This induces varying compliance vibrations in ball bearings. Using a simple bearing model, it is possible to evaluate variations of the bearing stiffness. In case only two balls are loaded, equations are simple:

$$Q_x = \sum_{j=1}^{2} f_j(t)\cos(\theta_j(t)) = F \tag{5}$$

$$Q_y = \sum_{j=1}^{2} f_j(t)\sin(\theta_j(t)) = 0 \tag{6}$$

The contact forces $f_j(t)$ are a function of the contact interference $\delta_j(t)$; therefore, the previous equations become:

$$Q_x = K\delta_1(t)^{3/2}\cos(\theta_1(t) + K\delta_2(t)^{3/2}\cos(\theta_2(t) = F \tag{7}$$

$$Q_y = K\delta_1(t)^{3/2}\sin(\theta_1(t) + K\delta_2(t)^{3/2}\sin(\theta_2(t) = 0 \tag{8}$$

The resolution of this system gives us the expression for δ_1 and δ_2. The stiffnesses of the bearing are then defined by the following expressions:

$$k_{xx} = \frac{\partial Q_x}{\partial x} = \frac{3}{2}F^{1/3}K^{2/3}f_x(\theta) \tag{9}$$

$$k_{yy} = \frac{\partial Q_y}{\partial x} = \frac{3}{2}F^{1/3}K^{2/3}f_y(\theta) \tag{10}$$

$$k_{xy} = k_{yx} = \frac{\partial Q_x}{\partial y} = \frac{\partial Q_y}{\partial x} = \frac{3}{2}F^{1/3}K^{2/3}f_{xy}(\theta) \tag{11}$$

These periodic functions in θ are detailed in Ref. [13]. The average values of the stiffness assume the average values of the resonance frequencies of the bearing. Of course because of the nonlinear behaviour strictly speaking no linear resonance frequency, as such, actually exists. However, some amplification of the vibrations appears around these frequencies leading to the wide use of the improper term "*resonance frequencies*":

$$f_x = \sqrt{\frac{k_{xx}}{M}}, \quad f_y = \sqrt{\frac{k_{yy}}{M}} \tag{12}$$

3. Experimental conditions

3.1. The test rig design

Predictable behaviour of the test rig is required and the design of the assembly is described in Fig. 2. An AC electric motor drives the first hydrodynamic spindle through a belt. A second horizontal hydrodynamic spindle is driven by a flexible coupling and supports the bearing. The rotor speed is easily controlled by the frequency of the electrical supply.

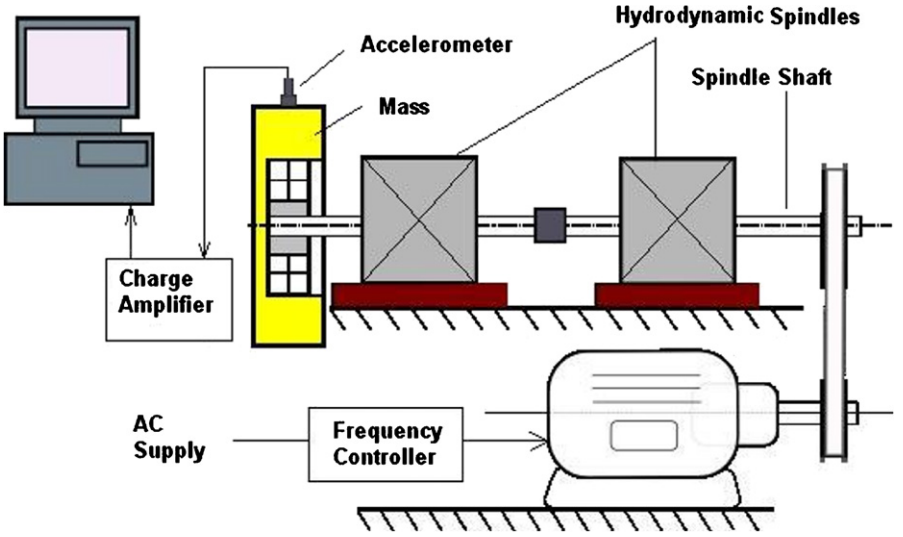

Fig. 2. Test rig equipment.

Table 1
Ball bearing parameters

Parameter	Value
Bearing pitch diameter	$D_p = 46.1\,\text{mm}$
Ball diameter	$D_b = 9.525\,\text{mm}$
Number of balls	$Z = 8\,\text{mm}$
Clearance	$e = 100\,\mu\text{m}$
Inner ring curvature	$R_i = 4.45\,\text{mm}$
Outer ring curvature	$R_e = 4.45\,\text{mm}$

Because of the hydrodynamic spindles, the lubricant is subject to radial loads and therefore the speed cannot be decreased below 500 rev/min, in order to prevent the shaft from stopping. The bearing outer ring is fitted in a free housing whose mass provides a constant vertical load applied to the system.

3.2. General settings

Internal bearing friction forces are very low and the mass inertia is sufficiently high and so the rotation of the outer ring around the bearing axis is not noticeable. The inner ring of the bearing is considered fixed except the rotation around its axis. The outer ring is assumed free except for the rotation around its axis. The rotor speed range was 500–3000 rev/min; the lower value is imposed by the spindles, the higher by the limitation of the drive motor.

To observe the unstable behaviour of the ball bearing, it is necessary to have an experimental set-up allowing one to excite the ball bearing at rotational speeds close to its resonance frequencies. This was not simple because of the limitations for the rotation speed and the static load. The following calculations describe the experiment. The ISO code of the ball bearing is 6206 and its main characteristics are given in Table 1.

A standard value of the Young's modulus of the balls and rings is considered. The Hertz theory gives a contact stiffness of $0.983610^{10}\,\text{N}\,\text{m}^{2/3}$. The rotor frequency and the ball pass frequency are linked by the following equation:

$$f_{pb} = Z\frac{f_i}{2}\left(1. - \frac{D_b}{D_p}\right) = 3.573 f_i \tag{13}$$

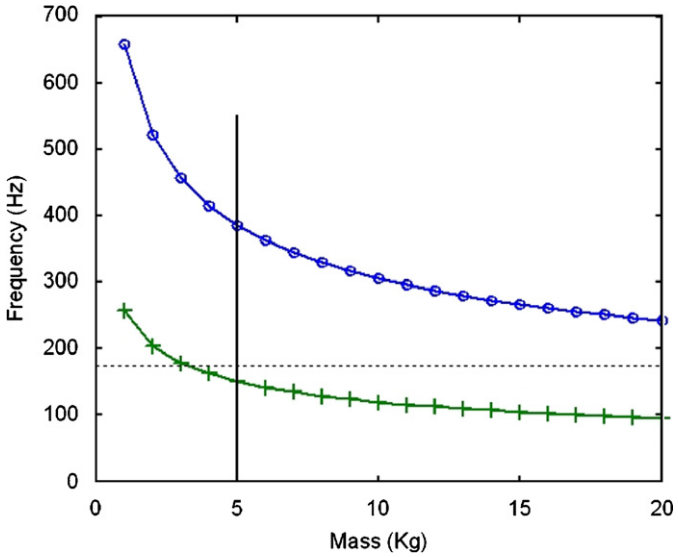

Fig. 3. Resonance frequencies f_x (○) and f_y (+) as a function of the mass added to the bearing.

Assuming that the radial load is equal to the weight of the mass M, one can calculate the static deflection (see Eqs. (13) and (14) in Ref. [7]) and the resonance frequencies of the mass-loaded ball bearing are:

$$f_x = \frac{658}{M^{1/3}}\ \text{Hz}, \quad f_y = \frac{258}{M^{1/3}}\ \text{Hz} \tag{14}$$

The frequency f_x corresponds to the motion in the direction of the vertical static load, and f_y to the vibration in the unloaded perpendicular direction. The mass M is added to the outer ring in order to lower the critical speeds to remain, within the range of 500–3000 rev/min; however, the loads applied to the spindles have to remain in an acceptable range. Fig. 3 illustrates the values of the resonant frequencies versus M. The frequencies f_x and f_y are given for masses below 10 kg, which is the maximum radial load acceptable for the test rig. The maximum value of the ball pass frequency f_{pb} is reached when the rotor speed is 3000 rev/min (i.e. 50 Hz):

$$(f_{pb})\text{max} = 3.573 \times 50 = 178.5\ \text{Hz} \tag{15}$$

The horizontal line indicates the higher value of the ball pass frequency f_{bp} max. When only 3 kg are added to the outer ring, f_{pb} reaches the first critical speed f_y but even for increased values of M up to the maximum possible limit, the f_{bp} max line remains below the second critical speed f_x. Therefore, the only sub-harmonic route to chaos is likely to occur in a 6206 bearing with an internal clearance of 100 μm and a mass of 5 kg added to the outer ring. This configuration is discussed in Section 5. To get within the range of the second critical speed, a modification of the assembly was necessary. The mass M was increased to 18 kg but was partially supported by a vertical spring; thereby, the radial static load applied to the bearing remains unchanged. This configuration is explored in Section 6. It is clear at this step that a complete quasi-periodic route to chaos cannot be reached with these settings: the maximum value of f_{pb} remains below f_x even for higher values of M; this indicates that the excitation frequency is not supposed to reach the second chaotic region.

4. Measurements and numerical treatments

4.1. Data acquisition

The bearing is centrally located in the housing M and the measurements are made on the outer diameter of the housing as shown in Fig. 4. The two piezo-accelerometers are attached to the mass; their directions are

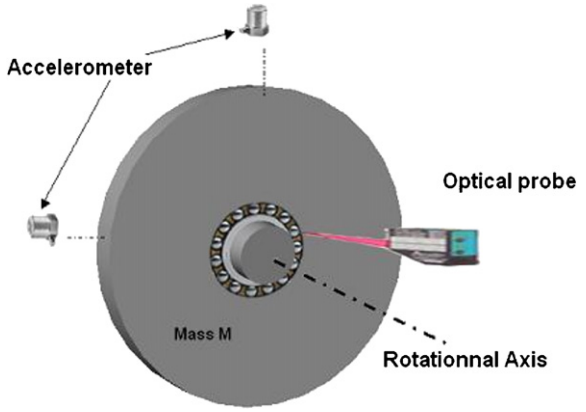

Fig. 4. Bearing and added mass: type and location of sensors.

chosen to be vertical and horizontal. One optical sensor is located facing the bearing. It is sensitive to the variation of light reflected by the balls.

The two piezo-accelerometers describe the motion of the bearing in its plane. The optical sensor generates a pulse at each pass of one ball with respect to a fixed point of the rig. This pulse is used as a trigger to sample x_e and y_e, the horizontal and vertical displacements that are used to build the attractors without taking into account the effect of irregularities.

Though it is a good quality bearing, the remaining geometrical imperfections of the raceways and the balls generate residual noise. The vertical $x_e(t)$ and horizontal $y_e(t)$ motions (response signal) get through a low-pass filter whose cut-off frequency is 400 and 1000 Hz (pulse signal). This operation was necessary to eliminate the signal noise.

4.2. Construction of Poincaré maps

The topological properties of attractors are independent of the phase plane used. Any degree of freedom of the assembly is convenient for the analysis of the dynamical behaviour. In this work, the phase portrait is built by using one motion of the bearing and its time derivative to obtain the corresponding Poincaré maps. Both signals are sampled at the ball pass frequency and then plotted one versus the other. Since no experimental device could perform all these functions, both velocity signal and pulse signals were transferred to a computer. Due to electronic considerations, each pulse is generated with a delay with respect to the ball pass. This phenomenon causes irregularities in the resulting attractor's projections. Therefore, a special numerical routine was developed to sample the vertical and horizontal motions of the bearing using an adjustable delay between pulses and the selection of samples. After some trials, a proper delay was chosen.

Fig. 5 illustrates the influence of filtering on a phase portrait and a Poincaré map. The original signal results are presented on the left, the phase portrait on the top and the Poincaré map on the bottom. On the right, the same signals after low pass frequency filtering are shown. This operation eliminates the high-frequency noise and gives a more comprehensible plot. The noise problem comes from the calculation of the signal time derivative, which is calculated numerically as a finite difference. Another difficulty encountered is the accuracy of the sampling process. Fig. 6 illustrates this point: a quasi-periodic attractor is in the centre which has been obtained with the proper sampling frequency. The plots on the right and left show the attractors resulting from a slight shift of 1 Hz in the sampling frequency. In both cases, the attractor is modified and becomes more complicated. Thus, the accuracy of the sampling is an important parameter. For periodic motions, the phenomenon is particularly sensitive because a slight shift in the sampling would result in a quasi-periodic attractor.

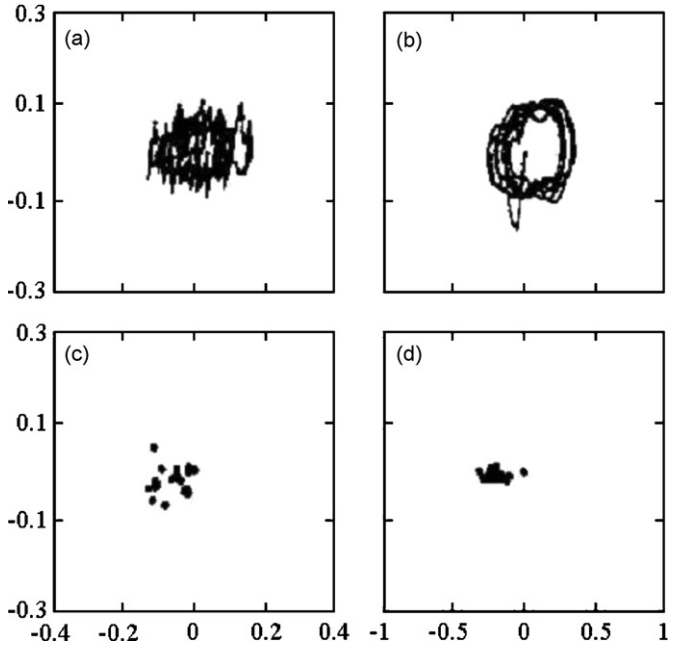

Fig. 5. Influence of low-pass filtering on phase portrait and Poincaré maps. Before filtering: (a) phase portrait, (c) Poincaré map; After filtering: (b) phase portrait, (d) Poincaré map.

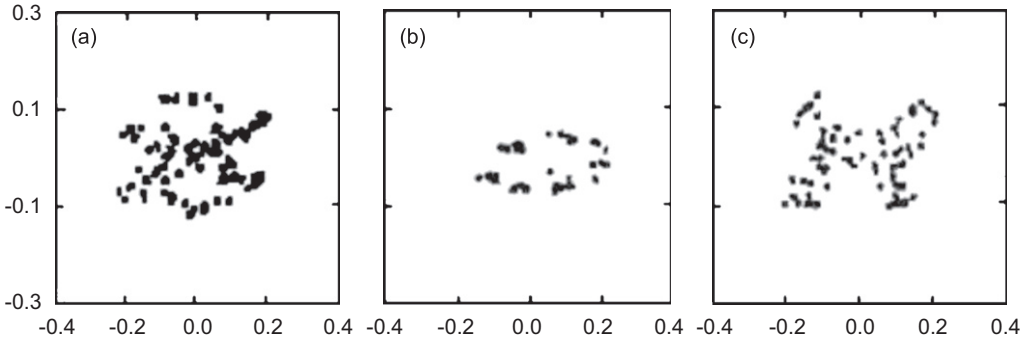

Fig. 6. Influence of a slight shift in the sampling frequency: (a) −1 Hz, (b) 0 Hz, (c) +1 Hz.

5. Internal resonance observation

In the previous paper [7], two routes to chaos were predicted and associated with internal resonances in the vertical and horizontal directions. To observe the experimental routes to chaos, it is important to set the internal resonances of the assembly in order to meet the theoretical predictions. A very simple design to observe the experimental resonances in the assembly is to consider the bearing motion at a low speed. Since the bearing clearance is large and the applied load is small, only a maximum of two balls is loaded. The periodic motion of the assembly is governed by the ball pass frequency. Each ball has two basic rotational degrees of freedom: the first speed is around its own z-axis and the second one is around the bearing z-axis. As the loading of one ball is removed for a short time only one ball remains loaded and supports the shaft. As this last ball moves on, the shaft falls on a new ball which then becomes loaded. This generates a large transition of the bearing stiffness, and the resulting transient motion shows the internal resonance frequencies of the system.

5.1. Horizontal resonance of the bearing

The horizontal resonance of the bearing can be observed in its horizontal motion. Fig. 7 presents a time history of the measured and calculated horizontal velocities. The ball pass period is clearly the basic period of the two curves. Inside each ball pass period, a limited number of decreasing oscillations is noticeable. These oscillations are characteristic of the horizontal resonance of the bearing. The obtained calculated signal is stable, showing constant amplitudes with time. Differences between theory and experiment exist; however, if averaged periods are considered, they agree quite well.

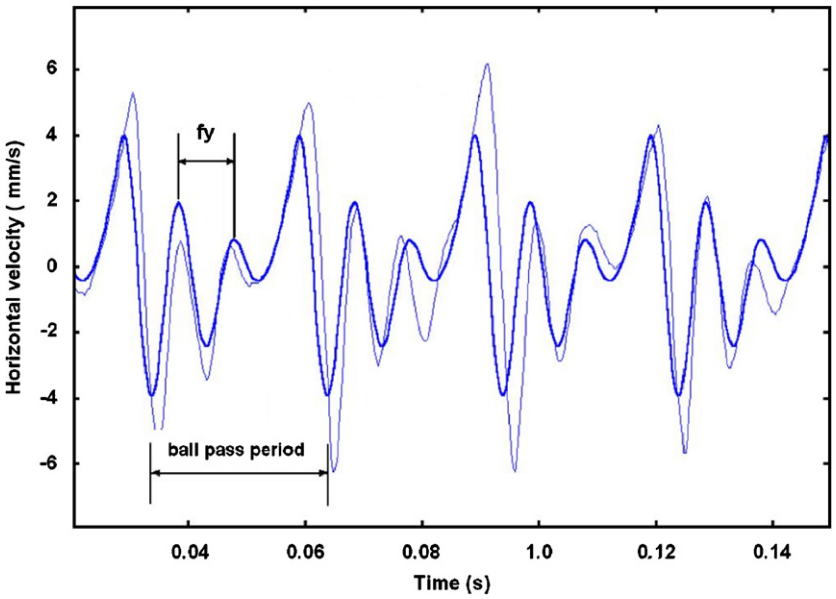

Fig. 7. Horizontal velocities; bearing type 6206J100 loaded with $M = 5\,\text{kg}$; rotation speed = 537 rev/min; experiments -, numerical –.

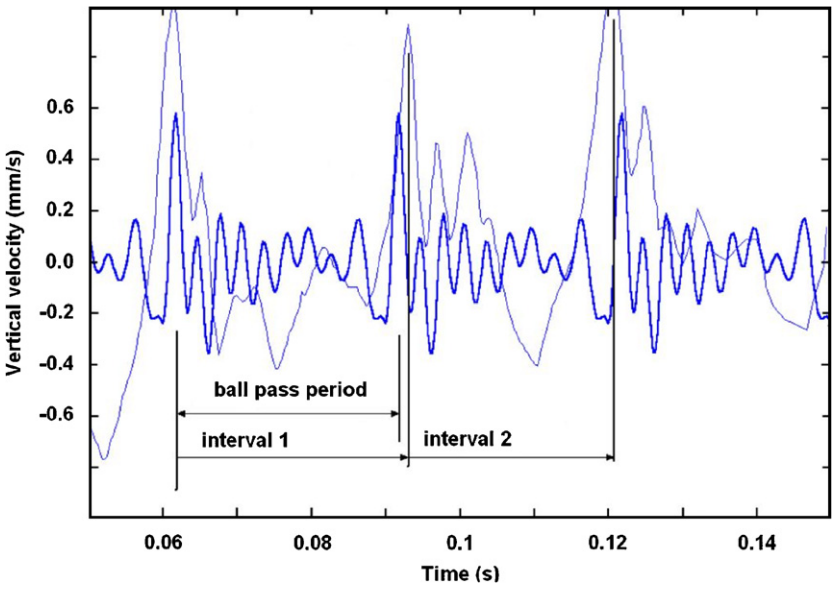

Fig. 8. Vertical velocities x; bearing type 6206J100 loaded with $M = 5\,\text{kg}$; rotation speed = 537 rev/min; experiments -, numerical –.

5.2. Vertical resonance of the bearing

The time history of the vertical motion is presented in Fig. 8. The measured signal is clearly subject to imperfection. The ball pass period is not constant and different observations show variations from −6% to +7% around an average value that is close to the theoretical value. Despite these imperfections in the measured signal, it is possible to make some observations. The ball pass is the basic period of the vertical speed. During each ball passage, some sub-oscillations take place. Their amplitudes are maximum after each peak of the ball pass and then decrease with time. It is possible to observe this slight change of the sub-oscillation period, explained by the continuous change in the bearing stiffness with the position of the balls. Theoretically, the period varies continuously from a minimum to a maximum. Using the experimental data, it is possible to extract the average value of the sub-oscillation frequencies in x (260 Hz) and y (370 Hz) directions.

6. The sub-harmonic route to chaos

6.1. Experimental settings

In the case of a non-suspended mass of 5 kg attached to the bearing, the first critical speed can be reached and the sub-harmonic route to chaos is predicted. The results are shown in Figs. 9 and 10. As mentioned in Section 2, the control parameter used to describe that route is the rotor speed. Fig. 9 presents the filtered time series, and Fig. 10 presents the corresponding phase portraits and Poincaré maps.

6.2. Experimental results

In the following, we introduce a notation that simplifies the comprehension of the observations: a sub-harmonic motion, characterised by a period whose value is n time that of the fundamental period of the excitation, will be defined as Tn.

At a low speed, ($n = 537$ rev/min), the motion is T1 periodic. Small oscillations between the large ones are due to the rotor falling on each new ball entering the bearing's loaded area zone. The phase portrait in Fig. 8 shows a complicated plot whose points are, however, close to each other. The corresponding Poincaré map on the right shows some points grouped in a limited area of the phase plane. In the perfect case, only one point could be seen but shaft vibrations make the points arrange in a close to point-like configuration.

When the rotor speed is 973 rev/min, the motion remains periodic T1 while the signal-to-noise ratio is better. The reason for this is not a modification of the geometrical properties of the assembly but a diminishing importance of the rotor collision. Each impact of the rotor on a new ball is tainted with randomness, and when the number of rotor rebounds is minimised, the random component of the motion decreases. Therefore, the Poincaré map in Fig. 10 contains very close points.

At $n = 1578$ rev/min, the time series show a periodic motion while the speed as well as the period of the motion has increased. This phenomenon betrays a bifurcation. In the frequency domain, the ball pass frequency is not the primary component of the motion since the sub-harmonic $f_{pb}/2$ has appeared. The motion is T2 periodic. The Poincaré map in Fig. 8 shows two spots of points.

At $n = 2082$ rev/min, the motion remains T2 periodic but the signal-to-noise ratio is higher and the Poincaré map shows two distinct groups of points. Getting near the first critical speed is characterised by an increase in amplitudes of the motions along the two axes.

When $n = 2183$, the sub-harmonic $f_{pb}/2$ governs the spectrum of the horizontal motion but noise has increased and therefore the Poincaré map is not very clear. The time series shows irregular amplitudes T2 periodically spaced. These irregularities in the time history reflect the noise present in the spectrum. Finally, when $n = 2754$ rev/min, the motion is again T1 periodic and the Poincaré map shows very close points. In the frequency domain, the ball pass frequency is the larger component but some noise is still present around the sub-harmonic $f_{pb}/2$. The time series shows a T1 periodic motion whereas the signal is not perfectly regular.

6.3. Simulation results

The theoretical time series presented in Fig. 9 are in good agreement with the experimental results, especially at low speeds. The phenomenon of bifurcation, which is experimentally observed at $n = 1578$ rev/min, is theoretically present at $n = 973$ rev/min with a T2 periodic motion. At $n = 2082$ rev/min, theoretical and experimental curves correspond and both show a T2 periodic motion. The experimental amplitudes are

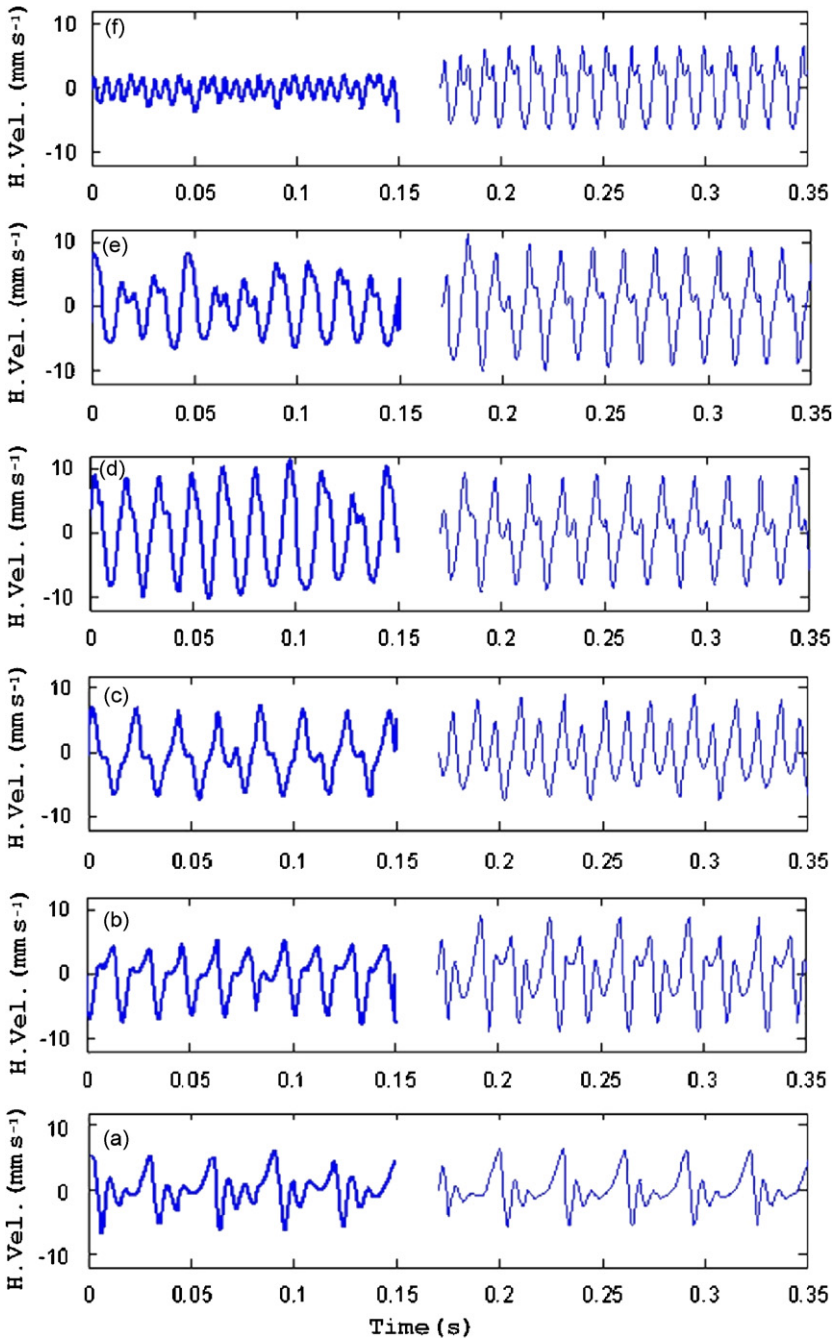

Fig. 9. Times series of the horizontal motion of the 6206J100 bearing loaded with $M = 5$ kg; $n = 537$(a), 973(b), 1578(c), 2082(d), 2183(e), 2754(f) rev/min.

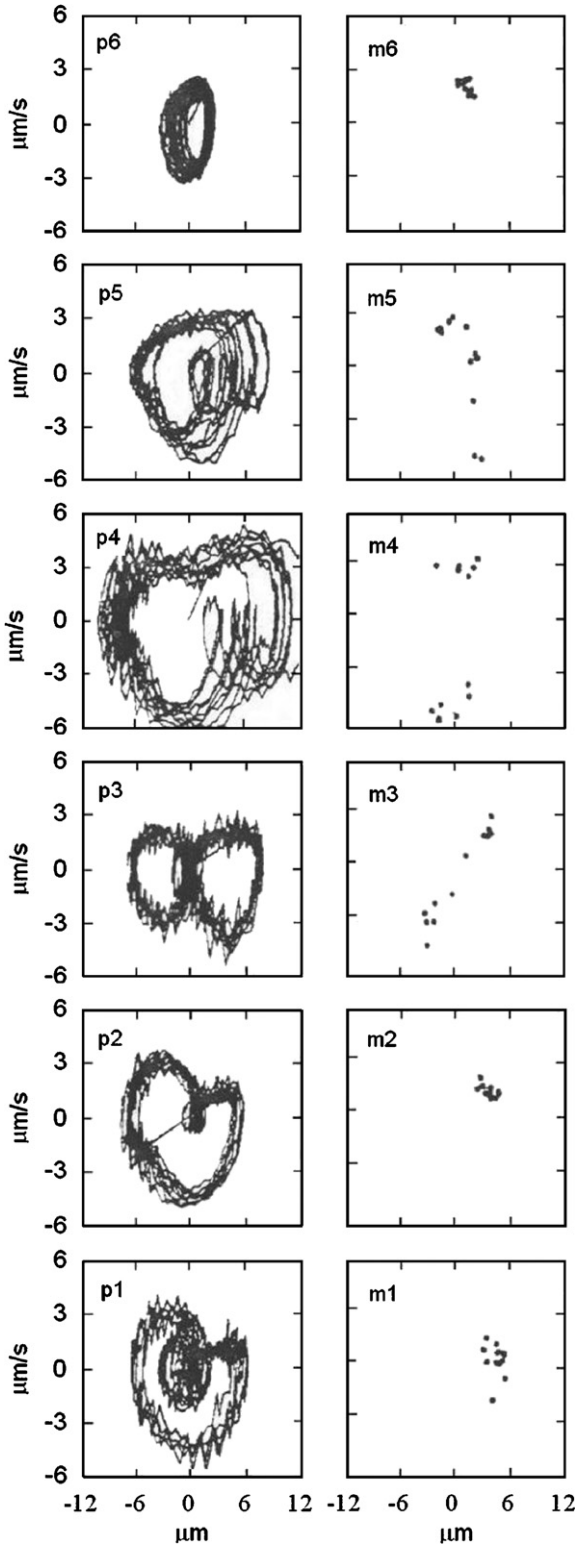

Fig. 10. Measured phase portrait (P) and Poincaré maps (M) in the (x_e, x'_e) phase plane. Bearing type 6206 loaded with $M = 5$ kg; $n = 537(1)$, $973(2)$, $1578(3)$, $2082(4)$, $2183(5)$, $2754(6)$ rev/min.

slightly higher; this applies to the maximum amplitude during one period, but also to the second peak during one period.

As the speed reaches 2754 rev/min, the theoretical motion remains T2 periodic, despite the experiment being T1 periodic. This indicates some limitations in our theoretical model.

This experiment confirms our theoretical prediction of a sub-harmonic route to chaos when the rotor speed reaches the first critical frequency. However, only the first bifurcation can be observed because the damping of the bearing is too high to allow other bifurcations to occur as suggested in Ref. [7].

7. The quasi-periodic route to chaos

7.1. Experimental settings

The mass added to the outer ring is increased to 18 kg and must be suspended as explained in Section 3. The second critical speed of the bearing should be around 3000 rev/min. As the rotor speed slowly increases from a low speed to its maximum value, the dynamic motion of the bearing changes and first describes a sub-harmonic route as shown previously, and then returns to a periodic motion before the occurrence of a bifurcation which results in a quasi-periodic motion. To characterise this quasi-periodic route to chaos of the bearing, the vertical motion is well adapted as it occurs around the resonance frequency of the vertical motion. Time series of the vertical speed are shown in Fig. 11, corresponding spectra in Fig. 12 and finally Poincaré maps in Fig. 13.

7.2. Experimental results

When $n = 1259$ rev/min, the spectrum shows two major peaks which are the ball pass frequency f_{bp} and a second one defined as f_w. Modulations are present but f_{bp} is clearly the main frequency.

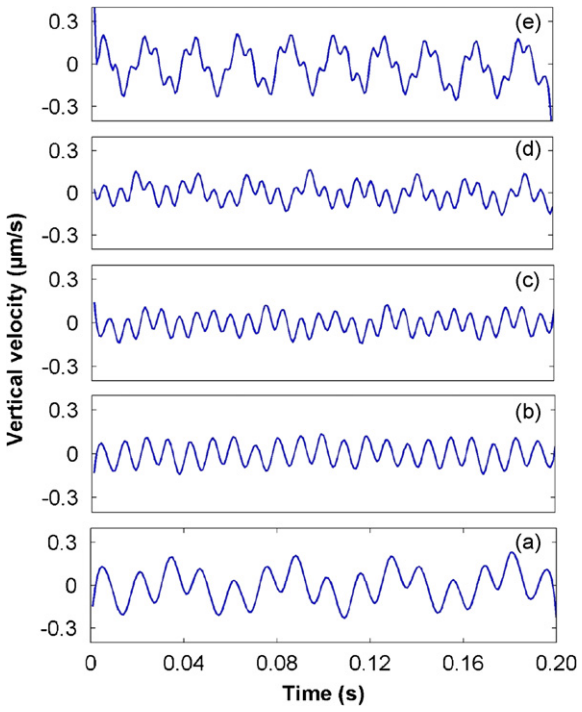

Fig. 11. Times series of the vertical motion of the 6206J100 bearing loaded with $M = 18$ kg; from bottom to top: $n = 1259$(a), 1797(b), 2267(c), 2485(d), 2905(e) rev/min.

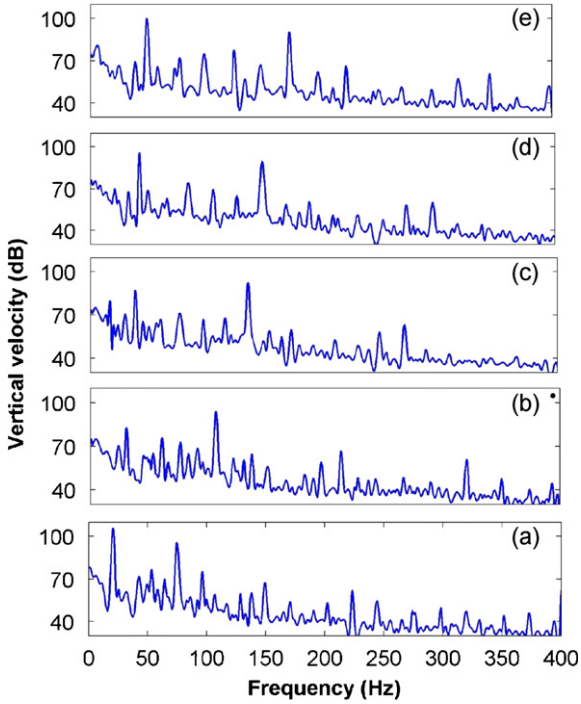

Fig. 12. Spectrum of the vertical motion of the 6206J100 bearing loaded with $M = 18$ kg; from bottom to top: $n = 1259$(a), 1797(b), 2267(c), 2485(d), 2905(e) rev/min.

At $n = 1797$ rev/min, the motion in time series seems to be almost controlled by the ball pass frequency. The spectrum shows a higher peak for f_{pb} than f_w.

When the speed is 2267 rev/min the time series shows a signal in which the f_{pb} frequency is easily noticeable. The Poincaré map is close to a single point.

When $n = 2485$ rev/min, the ratio f_w/f_{pb} is 1.035. The two frequencies f_{pb} and f_w govern the time series. The Poincaré section changes, and its size becomes larger, but no particular pattern is yet noticeable. The evolution of the motion is clearly noticeable when $n = 2905$ rev/min. The ratio is 1.09. At this time, the frequency f_w controls the motion, and f_{pb} is only noticeable in the small oscillations of the signal. The Poincaré map is very similar to a curve. The line is not continuous since the motion is quasi-periodic, and a long observation time would be necessary to complete the curve. The shape of the Poincaré section indicates that the second resonant speed of the bearing is very close. It was not possible to increase the speed of the rotor, and so the output of the second route to chaos could not be observed in this experiment.

7.3. Simulation results

The analysis of the theoretical simulations gives tendencies that can be compared to experiments.

At 1259, 1797 and 2267 speeds, the theoretical Poincaré maps show a finite number of points: respectively 4, 1 and 4 points. This is a characteristic of sub-harmonic motion. Experimentally the observation is not so clear because of the presence of noise in measured signals, but correlations are possible.

At $n = 1259$, the four points in the theoretical Poincaré map must be compared to the 4 small circles in the experimental Portrait de phase. These results are actually not very different, if the noise in measurements is taken into account. In the experiment, each small circle can be viewed as one point with uncertainty associated with the noise. Moreover, two circles are very close and can be seen as one point.

At $n = 1797$, the single point in the theoretical Poincaré map is to be compared to the two circles clearly noticeable in the experimental Portrait de phase.

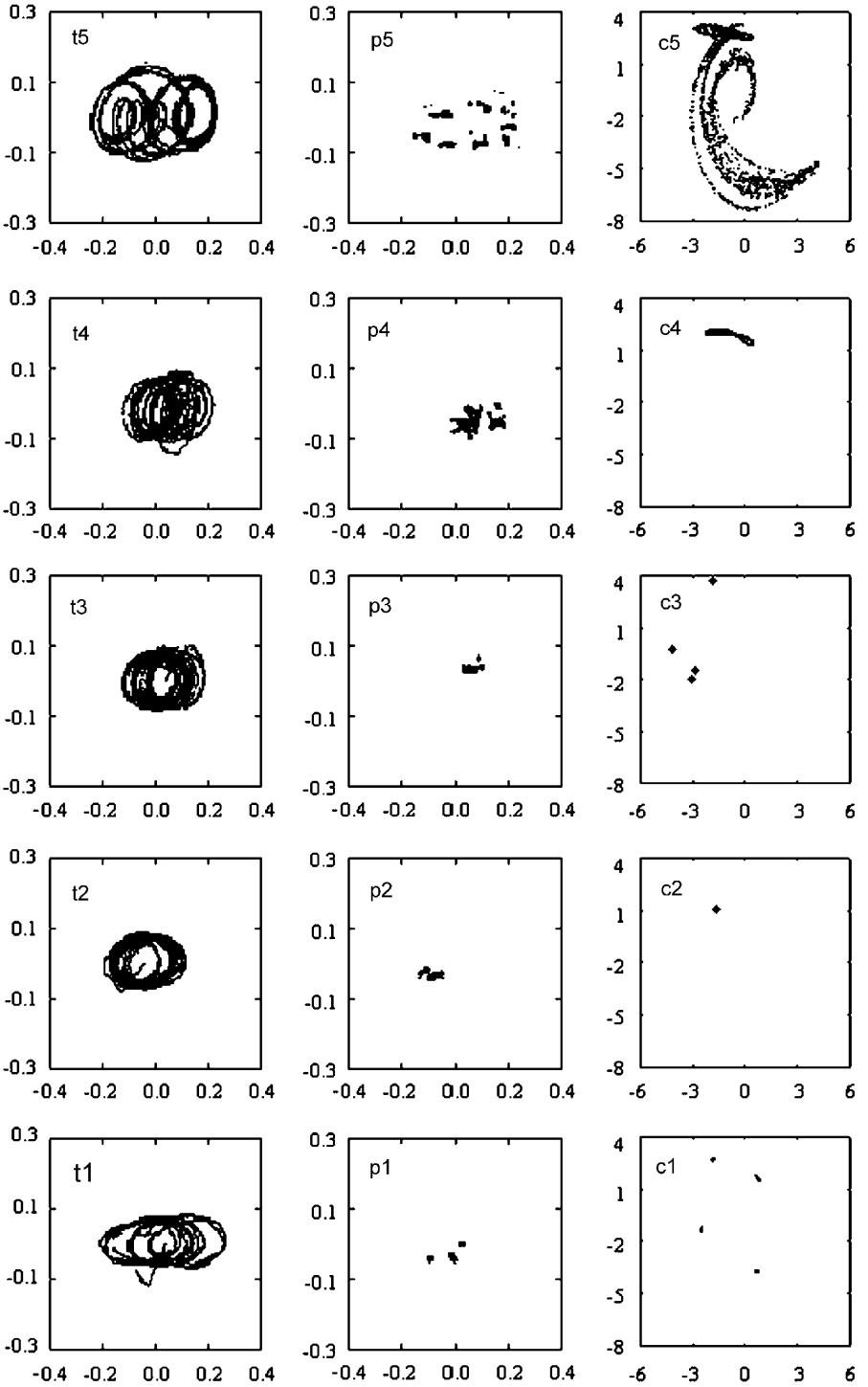

Fig. 13. Phase portrait and Poincaré maps of the 6206J100 bearing loaded with $M = 18$ kg; (t) experimental phase portrait in the (x'_e, x''_e) phase plane; (p) experimental phase portrait in the (x'_e, x''_e) phase plane; (c) numerical Poincaré maps in the (x'_e, x''_e) phase plane; $n = 1259(1), 1797(2), 2267(3), 2485(4), 2905(5)$ rev/min.

At higher rotation speeds, the theoretical attractor indicates a quasi-periodic motion and in the last case it probably indicates chaotic motion.

8. Conclusions

The existence of two different routes to chaos in a ball bearing dynamic motion has been experimentally observed. The first route is related to the horizontal resonant frequency of the bearing. Around this frequency, the system is unstable and generates some sub-harmonics of the excitation at the ball pass frequency.

Around the vertical "*resonance frequency*", a lower frequency f_w appears in the motion spectrum. Depending on the frequency ratio between f_{bp} and f_w, a sub-harmonic motion is noticeable, and in that case the order of the sub-harmonic motion depends on this ratio. As the speed reaches the second critical speed, the amplitude ratio between f_{bp} and f_w becomes close to 1 and results in a quasi-periodic motion. An interesting experimental observation is the quasi-periodic Poincaré map obtained at the highest possible speed of our rig.

Finally, the authors hope that this paper will encourage future work of this kind which will provide other experimental observations of routes to chaos in bearings.

References

[1] S.H. Ghafari, F. Golnaraghi, F. Ismail, Fault diagnosis based on chaotic vibration of rotor systems supported by ball bearings, in: *Proceedings of COMADEM 2006*, 2006, pp. 819–826.
[2] K. Fred, Choy, R. Wu, Damage identification of ball bearings for transmission systems in household appliances, *Tribology Transactions* 50 (2006) 74–81.
[3] C.S. Sunnersjo, Varying compliance of rolling bearings, *Journal of Sound and Vibration* 58 (1978) 363–373.
[4] S. Fukata, E.H. Gad, T. Kondou, T. Atabe, H. Tamura, On the radial vibration of a ball bearing, *Bulletin of the Japan Society of Mechanical Engineers* 28 (239) (1985) 899–904.
[5] T.C. Lim, R. Singh, Vibration transmission through rolling bearings, part 1: bearing stiffness formulation, *Journal of Sound and Vibration* 139 (1990) 179–199.
[6] A. Kahraman, R. Singh, Nonlinear dynamics of a geared rotor-bearing with multiple clearances, *Journal of Sound and Vibration* 144 (1991) 469–506.
[7] B. Mevel, J.L. Guyader, Routes to chaos in ball bearings, *Journal of Sound and Vibration* 162 (1993) 471–487.
[8] S.P. Harsha, Nonlinear dynamic of a high speed rotor supported by rolling element bearings, *Journal of Sound and Vibration* (2005) 1–36.
[9] F.C. Moon, *Chaotic Vibration*, Wiley-Interscience, New York, 1987.
[10] P. Berger, *L'Ordre dans la Chaos*, Hermann, Paris, 1988.
[11] W. Lautherborn, Methods of chaos physics and their applications acoustics, *Journal of the Acoustical Society of America* 84 (6) (1988) 1975–1993.
[12] M. Tiwari, K. Kupta, Dynamic response of an unbalanced rotor supported on ball bearings, *Journal of Sound and Vibration* 238 (5) (2000) 757–779.
[13] H. Tamura, Y. Tsuda, On the spring characteristics of a ball bearing, *Bulletin of J.S.M.E.* 23 (180) (1980) 961–969.